Effect of density and nucleon-nucleon potential on the fusion cross section within the relativistic mean field formalism

M. Bhuyan,[1,2,*] Raj Kumar,[3,†] Shilpa Rana,[3] D. Jain,[4] S. K. Patra,[5,6] and B. V. Carlson[7]

[1]*Department of Physics, Faculty of Science, University of Malaya, Kuala Lumpur 50603, Malaysia*
[2]*Institute of Research and Development, Duy Tan University, Da Nang 550000, Vietnam*
[3]*School of Physics and Materials Science, Thapar Institute of Engineering and Technology, Patiala 147004, India*
[4]*Department of Physics, Mata Gujri College, Fatehgarh, Punjab 140407, India*
[5]*Institute of Physics, Sachivalaya Marg, Sainik School, Bhubaneswar 751005, India*
[6]*Homi Bhabha National Institute, Anushakti Nagar, Mumbai 400085, India*
[7]*Instituto Tecnológico de Aeronáutica, São José dos Campos 12.228-900, São Paulo, Brazil*

(Received 14 January 2020; revised manuscript received 25 February 2020; accepted 12 March 2020; published 7 April 2020)

We have studied the effect of density and the nucleus-nucleus interaction potential on the fusion reaction cross section for the synthesis of heavy and superheavy nuclei within the relativistic mean field formalism. The double-folding procedure is used to obtain the nuclear interaction potential for the well-known M3Y and recently developed R3Y nucleon-nucleon potential for relativistic mean field densities. The NL3* parameter set is used to calculate the density distributions for targets and projectiles and is further used to obtain the nuclear potential. The ℓ-summed Wong formula is used to provide a transparent and analytic way to formulate the fusion cross sections for even-even ^{48}Ca + ^{154}Sm, ^{48}Ca + ^{238}U, ^{48}Ca + ^{248}Cm, ^{64}Ni + ^{238}U, ^{26}Mg + ^{248}Cm; even-odd ^{46}K + ^{181}Ta; and odd-odd ^{31}Al + ^{197}Au and ^{39}K + ^{181}Ta systems. The structural effects are also correlated with the fusion cross section through the equivalent diffuseness parameter using the densities of interacting nuclei for all nuclei (projects and targets) involved in the reactions just listed.

DOI: 10.1103/PhysRevC.101.044603

I. INTRODUCTION

At low energy, a large amount of information on fusion dynamics is available from experiments and theories, which mainly explains the fusion hindrance phenomenon, the neutron transfer effect, the effect of quasibound projectiles, breakup effects, synthesis of heavy and superheavy nuclei (SHN) away from the valley of stability, and prediction of the island of stability [1–22]. Furthermore, the fusion reactions also provide significant information in nuclear structure and vice versa. At present, the experimental emergence of hot and cold fusion reactions has dramatically renovated the formation or synthesis of exotic drip-line and superheavy nuclei in the laboratory [13–22]. Until now, the superheavy element with charge number $Z = 118$ has been produced via hot fusion reactions at the Joint Institute for Nuclear Research in Dubna, Russia (JINR) [23]. The formation of superheavy nuclei in experiments is extremely challenging [24–28]. To synthesize the neutron-rich heavy and superheavy nuclei (SHN), one can opt for neutron-rich radioactive beams, although the intensities of these beams are less than those of stable beams. Also, the properties of weakly bound nuclei and the isospin dependence of fusion reactions are prime elements for future experiments [29–40]. Furthermore, the estimation of fusion characteristics of heavy ions at extreme subbarrier energies is of great interest for understanding the reaction mechanisms in astrophysics and the synthesis of the superheavy nuclei [27,41,42].

In nuclear fusion, the nucleon-nucleon interaction is the key to a proper understanding of any nuclear phenomena because the nuclear structure effect enters mainly through this interaction. Theoretically, it is suggested that, below the Coulomb barrier, nuclear structure effects dominate the fusion dynamics, whereas the centrifugal potential suppresses structure effects at or above the barrier. However, the nuclear interaction part is not fully understood as yet. Thus, for a better understanding of the fusion reaction phenomenon, more accurate and microscopic methods for calculating the ion-ion interaction between the colliding nuclei should be exploited. In this work, we introduce the mean field nature of the heavy-ion reaction, namely, the mean field treatment of the nucleus-nucleus optical potential. At the mean field level, such an optical potential is readily obtained in the double-folding model [43–46] using the ground-state (g.s.) densities of the two colliding nuclei (projectiles and targets) and a realistic nucleon-nucleon (NN) interaction. This type of nucleus-nucleus optical potential has successfully explained many aspects of nuclear physics such as nuclear radioactivity, nuclear scattering, and nuclear fission and fusion process [10,47–49]. Recently, we have introduced a new effective NN

*bunuphy@um.edu.my
†rajkumar@thapar.edu

interaction, entitled the R3Y potential [10,47–49] analogous to the M3Y form [46] that can be derived from the relativistic mean field Lagrangian, which mainly depends on the relativistic force parameters, the coupling constant among the interacting mesons, and their masses [10,47–49]. In some of our previous works, we applied the R3Y potential to the study of the fusion hindrance phenomenon of the Ni-based reactions [10], namely, ^{64}Ni + ^{64}Ni, ^{64}Ni + ^{124}Sn, ^{64}Ni + ^{132}Sn, ^{58}Ni + ^{58}Ni, ^{58}Ni + ^{124}Sn, and ^{58}Ni + ^{132}Sn. We calculated the fusion cross section and their excitation functions for these even-even systems. From our previous investigations [10], we find that the R3Y interaction is in reasonably good agreement with the available experimental data as compare with the M3Y potential.

In this context, it will be of great interest to examine the performance of the relativistic R3Y potential along with the microscopic relativistic mean field density in terms of nuclear interaction potential for the study of fusion reaction for a variety of possible systems (even-even, even-odd, and odd-odd) at low energies. In the present analysis, we have chosen the lighter mass projectiles with heavier mass targets with possible combinations as even-even ^{48}Ca + ^{154}Sm, ^{48}Ca + ^{238}U, ^{48}Ca + ^{248}Cm, ^{64}Ni + ^{238}U, ^{26}Mg + ^{248}Cm; even-odd ^{46}K + ^{181}Ta; and odd-odd ^{31}Al + ^{197}Au and ^{39}K + ^{181}Ta systems. These systems are quite appropriate for the synthesis of exotic drip-line nuclei including superheavy, as well as for the astrophysical nucleosynthesis process. In addition, the understanding of extra driving energy from the barrier distribution may help to predict new possible ways of synthesizing heavy and superheavy nuclei [50]. As we mentioned above, the present analysis is a microscopic description of the interaction potential that incorporates the physical process, which can significantly influences the fusion process. To generate the nuclear potential, one needs to integrate an *NN* interaction over the matter distributions of the two colliding nuclei. Here the nuclear densities and nucleon-nucleon potential are obtained within the relativistic mean field formalism for the NL3* force parameter set. Parallel to the structural properties of the nuclei, the densities and potentials are slightly parameter dependent, which is reflected in the fusion properties as well. More details on various relativistic force parameters and their predictions can be found in Ref. [51] and references therein.

This paper is organized as follows: The relativistic mean field approach along with the double-folding procedure to generate the nucleus-nucleus potential will be discussed in Sec. II. The ℓ-summed Wong model will also be discussed in this section. Section III will be assigned to the discussion of the results obtained from our calculation. Finally, a summary and a brief conclusion will be given in Sec. IV.

II. RELATIVISTIC MEAN FIELD FORMALISM

The mean field treatment of quantum hadrodynamics (QHD) has been widely used to describe successfully nuclear structure and infinite nuclear matter properties [10,52–60]. In the relativistic mean field approach, the nucleus is considered as a composite system of nucleons interacting through the exchange of mesons and photons [53,61–65]. We use the microscopic self-consistent relativistic mean field (RMF) theory as a standard tool to investigate the fusion characteristics via the ℓ-summed Wong model. The form of a typical relativistic Lagrangian density for a nucleon-meson many-body system is [52,53,57,58,60–68]

$$\begin{aligned}\mathcal{L} = {} & \overline{\psi}\{i\gamma^{\mu}\partial_{\mu} - M\}\psi + \frac{1}{2}\partial^{\mu}\sigma\,\partial_{\mu}\sigma \\ & -\frac{1}{2}m_{\sigma}^{2}\sigma^{2} - \frac{1}{3}g_{2}\sigma^{3} - \frac{1}{4}g_{3}\sigma^{4} - g_{s}\overline{\psi}\psi\sigma \\ & -\frac{1}{4}\Omega^{\mu\nu}\Omega_{\mu\nu} + \frac{1}{2}m_{w}^{2}\omega^{\mu}\omega_{\mu} - g_{w}\overline{\psi}\gamma^{\mu}\psi\omega_{\mu} \\ & -\frac{1}{4}\vec{B}^{\mu\nu}\cdot\vec{B}_{\mu\nu} + \frac{1}{2}m_{\rho}^{2}\vec{\rho}^{\,\mu}\cdot\vec{\rho}_{\mu} - g_{\rho}\overline{\psi}\gamma^{\mu}\vec{\tau}\psi\cdot\vec{\rho}^{\,\mu} \\ & -\frac{1}{4}F^{\mu\nu}F_{\mu\nu} - e\overline{\psi}\gamma^{\mu}\frac{(1-\tau_{3})}{2}\psi A_{\mu}. \end{aligned} \tag{1}$$

The ψ are the Dirac spinors of the nucleons. Here g_{σ} (m_{σ}), g_{ω} (m_{ω}), and g_{ρ} (m_{ρ}) are the coupling constants (masses) for the σ, ω, and ρ mesons, respectively. The isospin and the third component of the isospin are denoted τ and τ_3, respectively. The constants g_2, g_3, and $\frac{e^2}{4\pi}$ are the coupling constants for self-interacting nonlinear σ-meson field and photon, respectively. The quantities A_{μ} and M stand for the electromagnetic field and the mass of the nucleon, respectively. The vector field tensors for the ω^{μ}, $\vec{\rho}_{\mu}$, and photon are given by

$$F^{\mu\nu} = \partial_{\mu}A_{\nu} - \partial_{\nu}A_{\mu}, \tag{2}$$

$$\Omega_{\mu\nu} = \partial_{\mu}\omega_{\nu} - \partial_{\nu}\omega_{\mu}, \tag{3}$$

$$\vec{B}^{\mu\nu} = \partial_{\mu}\vec{\rho}_{\nu} - \partial_{\nu}\vec{\rho}_{\mu}, \tag{4}$$

respectively. From the above Lagrangian density we obtain the field equations for the Dirac nucleons and the mesons (i.e., σ, ω, and ρ, field) as

$$\begin{aligned} & [-i\alpha\cdot\nabla + \beta(M + g_{\sigma}\sigma) + g_{\omega}\omega + g_{\rho}\tau_{3}\rho_{3}]\psi = \epsilon\psi, \\ & \left(-\nabla^{2} + m_{\sigma}^{2}\right)\sigma(r) = -g_{\sigma}\rho_{s}(r) - g_{2}\sigma^{2}(r) - g_{3}\sigma^{3}(r), \\ & \left(-\nabla^{2} + m_{\omega}^{2}\right)V(r) = g_{\omega}\rho(r), \\ & \left(-\nabla^{2} + m_{\rho}^{2}\right)\rho(r) = g_{\rho}\rho_{3}(r). \end{aligned} \tag{5}$$

In the limit of one-meson exchange, for a static baryonic medium, the single nucleon-nucleon potentials for scalar (σ), and vector (ω, ρ) fields are given by [48,69,70],

$$\begin{aligned} V_{\sigma} = {} & -\frac{g_{\sigma}^{2}}{4\pi}\frac{e^{-m_{\sigma}r}}{r} + \frac{g_{2}^{2}}{4\pi}re^{-2m_{\sigma}r} + \frac{g_{3}^{2}}{4\pi}\frac{e^{-3m_{\sigma}r}}{r}, \\ V_{\omega}(r) = {} & +\frac{g_{\omega}^{2}}{4\pi}\frac{e^{-m_{\omega}r}}{r}, \quad V_{\rho}(r) = +\frac{g_{\rho}^{2}}{4\pi}\frac{e^{-m_{\rho}r}}{r}. \end{aligned} \tag{6}$$

The total effective *NN* interaction is obtained from the scalar and vector parts of the meson fields. A recently developed relativistic *NN* interaction potential analogous to the M3Y form [46] is entitled the R3Y potential. The relativistic effective nucleon-nucleon interaction $V_{\rm eff}^{\rm R3Y}$ for the NL3* force

including the single-nucleon exchange effect as [10,46–49]

$$V_{\rm eff}^{\rm R3Y}(r) = \frac{g_\omega^2}{4\pi}\frac{e^{-m_\omega r}}{r} + \frac{g_\rho^2}{4\pi}\frac{e^{-m_\rho r}}{r} - \frac{g_\sigma^2}{4\pi}\frac{e^{-m_\sigma r}}{r} + \frac{g_2^2}{4\pi} r e^{-2m_\sigma r} + \frac{g_3^2}{4\pi}\frac{e^{-3m_\sigma r}}{r} + J_{00}(E)\delta(r). \quad (7)$$

On the other hand, the M3Y effective interaction, obtained from a fit of the G-matrix elements based on the Reid-Elliott soft-core NN interaction [46], in an oscillator basis, is the sum of three Yukawa terms (M3Y) with a long-range tail of the one-pion exchange potential (OPEP). The widely used M3Y effective interaction $V_{\rm eff}^{\rm M3Y}(r)$ is given by

$$V_{\rm eff}^{\rm M3Y}(r) = 7999\frac{e^{-4r}}{4r} - 2134\frac{e^{-2.5r}}{2.5r} + J_{00}(E)\delta(r), \quad (8)$$

where the ranges are in fm and the strengths in MeV. More details of Eqs. (7) and (8) can be found in Refs. [10,47,48,69,70]. The nuclear interaction potential $V_n(R)$ between the projectile (p) and the target (t) nuclei, with the respective RMF (NL3*) calculated nuclear densities ρ_p and ρ_t, is

$$V_n(\vec{R}) = \int \rho_p(\vec{r}_p)\rho_t(\vec{r}_t)V_{\rm eff}(|\vec{r}_p - \vec{r}_t + \vec{R}| \equiv r)d^3r_p d^3r_t, \quad (9)$$

obtained by using the well-known double-folding procedure [46] for the M3Y and the relativistic R3Y interaction potential, proposed in Refs. [10,47,48], supplemented by a zero-range pseudopotential representing the single-nucleon exchange effects. Adding the Coulomb potential $V_C(R)$ $(=Z_pZ_te^2/R)$ with the nuclear interaction potential $V_n(R)$ [obtained from Eq. (9)] results the total nuclear interaction potential $V_T(R)$ [10,47,48], which will be used for fusion study within the ℓ-summed Wong model in the preceding section. As we know, pairing plays an important role in the nuclear bulk properties, including the density distribution of open-shell nuclei. Hence, we consider the BCS pairing approach to account for pairing correlation in the present analysis and also use a blocking procedure to take care of the odd-A and odd-odd nuclei [57–59,71,72].

Fusion cross section in terms of partial waves

Wong established a formula [73] to study the possible formation of a compound nucleus (CN), and it was further extended by Gupta and collaborators by carrying out the actual summation over ℓ partial waves [74]. The fusion cross section for two colliding spherical nuclei with center-of-mass energy $E_{\rm c.m.}$ in terms of ℓ partial waves is given by [73]

$$\sigma(E_{\rm c.m.}) = \frac{\pi}{k^2}\sum_{\ell=0}^{\ell_{\rm max}}(2\ell+1)P_\ell(E_{\rm c.m.}), \quad (10)$$

with $k = (\frac{2\mu E_{\rm c.m.}}{\hbar^2})^{1/2}$ and μ being the reduced mass. P_ℓ is the transmission coefficient for each ℓ which describes the penetration of barrier $V_T^\ell(R)$, which is given by

$$V_T^\ell(R) = V_n(R, A_i) + V_C(R, Z_i) + \frac{\hbar^2\ell(\ell+1)}{2\mu R^2}. \quad (11)$$

Here, $\ell_{\rm max}$ is the maximum value that the angular momentum contributes to the fusion cross section $\sigma_{\rm fus}(mb)$. In the present work, the $\ell_{\rm max}$ values are obtained from the sharp cutoff model [75] for energies above the barrier and are extrapolated for below-barrier energies.

Using the Hill-Wheeler [76,77] approximation, the penetrability P_ℓ in terms of its barrier height $V_B^\ell(E_{\rm c.m.})$ and curvature $\hbar\omega_\ell(E_{\rm c.m.})$ is

$$P_\ell = \left(1 + \exp\left\{\frac{2\pi\left[V_B^\ell(E_{\rm c.m.}) - E_{\rm c.m.}\right]}{\hbar\omega_\ell(E_{\rm c.m.})}\right\}\right)^{-1}, \quad (12)$$

with $\hbar\omega_\ell$ evaluated at the barrier position $R = R_B^\ell$ corresponding to the barrier height V_B^ℓ, which is given as

$$\hbar\omega_\ell(E_{\rm c.m.}) = \hbar\left[\left|d^2V_T^\ell(R)/dR^2\right|_{R=R_B^\ell}/\mu\right]^{1/2}, \quad (13)$$

with R_B^ℓ obtained from the condition

$$\left|dV_T^\ell(R)/dR\right|_{R=R_B^\ell} = 0.$$

The Hill-Wheeler approximation assumes the interaction barrier to be parabolic, which leads to the analytical expression for the transmission and is widely used in the fusion reactions of heavy ions. However, for the case of asymmetric reactions, the potential deviates from the inverted oscillator even near the barrier. More details can be found in Refs. [78–80]. Since it is a widely used approximation, and hence for the comparison, we also adopted the same.

Instead of solving Eq. (10) explicitly, which requires the complete ℓ-dependent potentials $V_T^\ell(R)$, Wong [73] carried out the ℓ summation in Eq. (10) *approximately* under specific conditions

(i) $\hbar\omega_\ell \approx \hbar\omega_0$ and
(ii) $V_B^\ell \approx V_B^0 + \frac{\hbar^2\ell(\ell+1)}{2\mu R_B^{0^2}}$,

which assumes $R_B^\ell \approx R_B^0$ also. In other words, both V_B^ℓ and $\hbar\omega_\ell$ are obtained for the $\ell = 0$ case. Using these approximations, and replacing the ℓ summation in Eq. (10) by an integral, gives, upon integration, the $\ell = 0$ barrier-based Wong formula [73],

$$\sigma(E_{\rm c.m.}) = \frac{R_B^{0^2}\hbar\omega_0}{2E_{\rm c.m.}}\ln\left\{1 + \exp\left[\frac{2\pi}{\hbar\omega_0}\left(E_{\rm c.m.} - V_B^0\right)\right]\right\}. \quad (14)$$

This is the simple formula to calculate the fusion cross section by using the barrier characteristics V_B^0, R_B^0, and $\hbar\omega_0$ within the barrier-penetration model for spherical nuclei. However, Wong's specific ℓ-summation procedure, leading to the use of only the $\ell = 0$ barrier, excludes modifications entering the potential due to its ℓ dependence. For details see Ref. [74]. So a more precise formula, as given in Eq. (10), with penetrability P_ℓ given by Eqs. (12) and (13), is employed in the present work for calculating the fusion cross section.

III. CALCULATION AND DISCUSSIONS

The RMF calculations furnish principally basic nuclear structure properties such as the binding energy, root-mean-square radius (proton, charge, and neutron), quadrupole

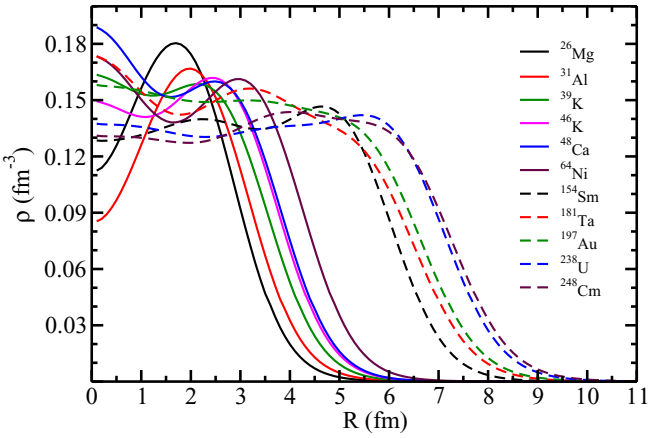

FIG. 1. The RMF (NL3*) total radial density distribution for projectiles (solid line) ^{26}Mg, ^{31}Al, ^{39,46}K, ^{48}Ca, and ^{64}Ni nuclei and targets ^{154}Sm, ^{181}Ta, ^{197}Au, ^{238}U, and ^{248}Cm nuclei. See text for details.

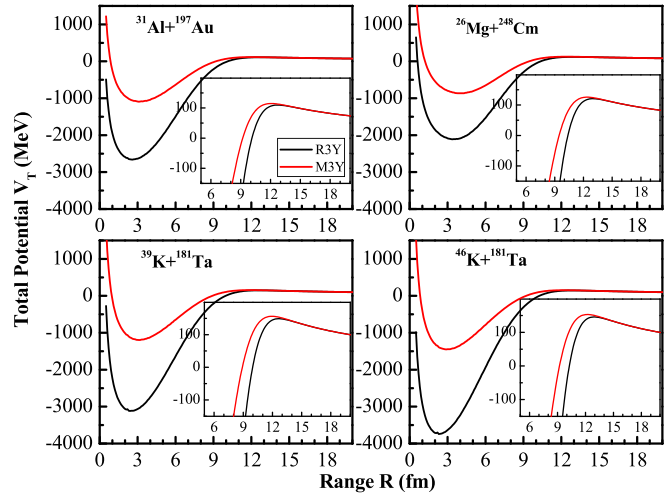

FIG. 2. The total nuclear potential $V_T(R)$ for odd-odd $^{31}\mathrm{Al}+^{197}\mathrm{Au}$, $^{39}\mathrm{K}+^{181}\mathrm{Ta}$; even-even $^{26}\mathrm{Mg}+^{248}\mathrm{Cm}$; and even-odd $^{46}\mathrm{K}+^{181}\mathrm{Ta}$ systems using the phenomenological M3Y (solid black line) and relativistic R3Y (solid red line) nucleon-nucleon potentials as a function of radial separation R. See text for more details.

moment Q_{20}, the total density distribution (i.e., the sum of the proton and neutron densities), and the single-particle energy level for nucleons. To study the fusion hindrance phenomenon by using the self-consistent relativistic mean field formalism via the $\ell_{\max}$-summed Wong model, we need the nuclear density distribution of the interacting nuclei (projectile and target nucleus) and the nucleon-nucleon potential, which are obtained from the relativistic mean field Lagrangian. Here, we use spherical densities for the target (t) and projectile (p) as the input to estimate the nucleus-nucleus interaction potential using Eq. (9). Many other studies have already adopted the densities from a well-defined mean field model and folded them with a phenomenological nucleon-nucleon (NN) interaction to obtain a nuclear interaction potential [81–85]. Here we introduce the relativistic NN potential from the relativistic Lagrangian by solving the field equations in Eq. (5) for the interacting mesons to obtain the nucleus-nucleus interaction potential. This kind of relativistic NN-potential (so-called R3Y potential) has been successfully applied in some of our recent works for the study of the radioactive decay process [47–49]. It is worth mentioning that we also applied this R3Y potential in the fusion study for selected Ni-based reactions [10]. The present work is of great interest to apply R3Y potential for fusion studies of various systems. In Fig. 1, we have shown the total density distributions for interacting projectiles (solid line) and targets (dashed line) obtained from the NL3* parameter set as a function of radius. From the figure, one finds that the central density is a bit smaller in magnitude and enhanced a little towards the surface region, due to Coulomb repulsion in case of projectiles, which is a very general feature in the light-mass nuclei.

A. Nucleus-nucleus optical potential

The nuclear interaction potential $\mathrm{V}_n(R)$ between the projectile (p) and target (t) nuclei is calculated by using the well-known double-folding procedure in Eq. (9) [46,47] using the RMF densities ρ_p and ρ_t for the phenomenological M3Y and recently developed relativistic R3Y NN potential. The R3Y potential can be obtained either analytically or numerically for many relativistic parameter sets, as it obtains from the masses and coupling constants of the interacting meson fields, where an effective Lagrangian describes the interaction among the nucleons through the effective mesons and electromagnetic fields. Here, the R3Y interaction is obtained for the NL3* parameter set for the analysis [10]. It is worth mentioning that the R3Y interaction potential has already been applied to radioactivity studies of several highly isospin asymmetry systems using a preformed cluster decay model (PCM) [47–49] and very recently to the fusion hindrance of Ni-based systems [10].

The total nuclear interaction potential $\mathrm{V}_T(R) = \mathrm{V}_n(R) + \mathrm{V}_C(R)$ is obtained for the even-even $^{48}\mathrm{Ca}+^{154}\mathrm{Sm}$, $^{48}\mathrm{Ca}+^{238}\mathrm{U}$, $^{48}\mathrm{Ca}+^{248}\mathrm{Cm}$, $^{64}\mathrm{Ni}+^{238}\mathrm{U}$, $^{26}\mathrm{Mg}+^{248}\mathrm{Cm}$; even-odd $^{46}\mathrm{K}+^{181}\mathrm{Ta}$; and odd-odd $^{31}\mathrm{Al}+^{197}\mathrm{Au}$ and $^{39}\mathrm{K}+^{181}\mathrm{Ta}$ systems, where V_n and V_C stand for the nuclear and Coulomb potentials, respectively. The total interaction potentials for the R3Y (solid red line) and M3Y (solid black line) potential for all the systems are displayed in Figs. 2 and 3 for comparison. The fusion barrier heights of M3Y and R3Y potentials are also tabulated in Table I. The Bass barriers are also given for the comparison. From the figures, we note that $\mathrm{V}_T(R)$ follows a similar pattern for both R3Y and M3Y NN interactions. The difference in the total potential V_T is due to the difference of the nucleon-nucleon potential, which is reflected through V_n, because the Coulomb potential is independent of the nucleon-nucleon interaction potential of choice. The nuclear potentials V_n for M3Y and R3Y differ significantly in the central region and this difference decreases gradually as the radial separation increases. Furthermore, the height of the barrier for the M3Y NN interaction is slightly higher than that of the R3Y case (more clearly seen in the inset

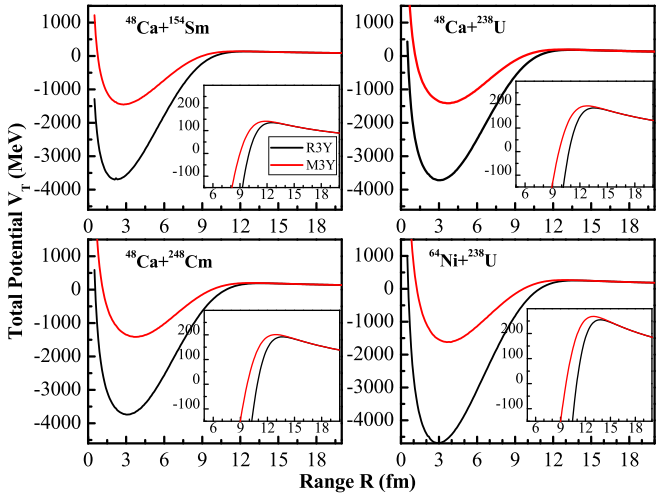

FIG. 3. Same as Fig. 2, but for even-even ^{48}Ca + ^{154}Sm, ^{48}Ca + ^{238}U, ^{48}Ca + ^{248}Cm, and ^{64}Ni + ^{238}U systems. See text for more details.

figures). Thus, the barrier height from R3Y is more attractive than the M3Y interaction, which will be reflected in the fusion characteristics.

B. Fusion cross sections

To estimate the fusion reaction cross section, we need the barrier characteristics such as barrier height, position, and frequency. These inputs can be extracted from the total interaction potential of colliding nuclei [see Eq. (11)]. In our recent work [10], it is observed that the comparison of calculated cross sections with experimental data is better if ℓ-summed Wong model is considered as compared with the Wong formula. So in this work, the ℓ-summed Wong formula [see Eq. (10)] is used to obtain the fusion reaction cross section for even-even ^{48}Ca + ^{154}Sm, ^{48}Ca + ^{238}U, ^{48}Ca + ^{248}Cm, ^{64}Ni + ^{238}U, ^{26}Mg + ^{248}Cm; even-odd ^{46}K + ^{181}Ta; and odd-odd ^{31}Al + ^{197}Au and ^{39}K + ^{181}Ta systems. The $\ell_{\max}$ values are extracted by using the sharp cutoff model [75] for energies above the barrier and are extrapolated for lower energies by using the above-barrier $\ell_{\max}$ values as a function of center-of-mass energy.

TABLE I. Calculated barrier heights for M3Y and R3Y potentials compared with Bass barriers used in the experimental works for ^{48}Ca + ^{154}Sm, ^{48}Ca + ^{238}U, ^{48}Ca + ^{248}Cm, ^{64}Ni + ^{238}U, ^{26}Mg + ^{248}Cm, ^{46}K + ^{181}Ta, ^{31}Al + ^{197}Au, and ^{39}K + ^{181}Ta systems [33–36].

	Barrier height (MeV)		
Reactions	M3Y	R3Y	Bass [33–36]
^{31}Al + ^{197}Au	114.83	109.75	115.2
^{39}K + ^{181}Ta	156.24	148.85	157.5
^{46}K + ^{181}Ta	153.11	145.79	154.0
^{26}Mg + ^{248}Cm	125.83	120.77	129.0
^{48}Ca + ^{154}Sm	141.26	134.768	141.0
^{48}Ca + ^{248}Cm	200.82	191.61	202.0
^{48}Ca + ^{238}U	194.20	185.36	195.0
^{64}Ni + ^{238}U	268.14	254.70	267.5

In Fig. 4, the solid red and black lines are for the fusion cross section using the relativistic R3Y interaction and the phenomenological M3Y potential, respectively. The experimental data [33–38] are also given for comparison, wherever available. From the figure, it is observed that R3Y performs relatively better than the M3Y interaction experimental data [33–38] at below-barrier energies. In other words, the cross section corresponding to R3Y almost overlap with the experimental data except in a few cases for energies below the Coulomb barrier, whereas the M3Y fits the data only at above-barrier energies. The nuclear interaction from R3Y potential explains the cross section reasonably well at comparatively lower energies. It is to be noted that the fusion cross section corresponding to the R3Y interaction is always larger compared with that of the M3Y potential. It is observed from all these systems (see Fig. 4) that the R3Y interaction is proven to be a relatively better choice than M3Y for considering the fusion reactions below the barrier at low energies. This is due to the slightly lower barrier peak and internal depth of the nuclear potential V_n of the R3Y potential.

C. Equivalent diffuseness parameter

In the case of even-even ^{26}Mg + ^{248}Cm and ^{48}Ca + ^{238}U and odd-odd ^{39}K + ^{181}Ta systems, the cross sections from the R3Y potential are a little different from the experimental data at below-barrier energies. To correlate this deviation with the density distribution, we calculate the equivalent diffuseness parameter for all interacting (projectiles and targets) nuclei. An equivalent diffuseness parameter a_i can be obtained by using the relation, $a_i \approx -\rho_i(r)/\frac{d\rho_i}{dr}$, where i stands for neutron- (a_n), proton- (a_p), and charge-density (a_{ch}) distributions. The results of the equivalent diffuseness parameter for neutron and proton density from the relativistic mean field approach for the NL3* parameter set are shown in Fig. 5 along with equivalent experimental values [86,87]. The experimental diffuseness parameters are obtained for charge-density distributions extracted from electron scattering [86,87]. From Fig. 5, one observes that the diffuseness values for the experimental charge distributions vary around an average of $\approx 0.52 \pm 0.02$ fm, which is larger than the calculated values for proton distributions. The average diffuseness values for the experimental charge a_{ch} and calculated proton diffuseness a_p are 0.52 ± 0.02 and 0.44 ± 0.04 fm, respectively. The difference between a_{ch} (from the experimental charge distribution) and a_p (from the calculated proton distribution) is around $\sim$0.08 because the effective charge radius of the proton is not considered in the proton-density distribution. The reaction systems associated with a large standard deviation in a_p values show a difference at below-barrier energy in the cross section. For example, for the reaction systems, ^{26}Mg + ^{248}Cm, ^{48}Ca + ^{238}U, and ^{39}K + ^{181}Ta, we find that the calculated results slightly underestimate the experimental data. Analogous to the cross sections, we also find a deviation in a_p for associated reaction systems. Hence, the structural

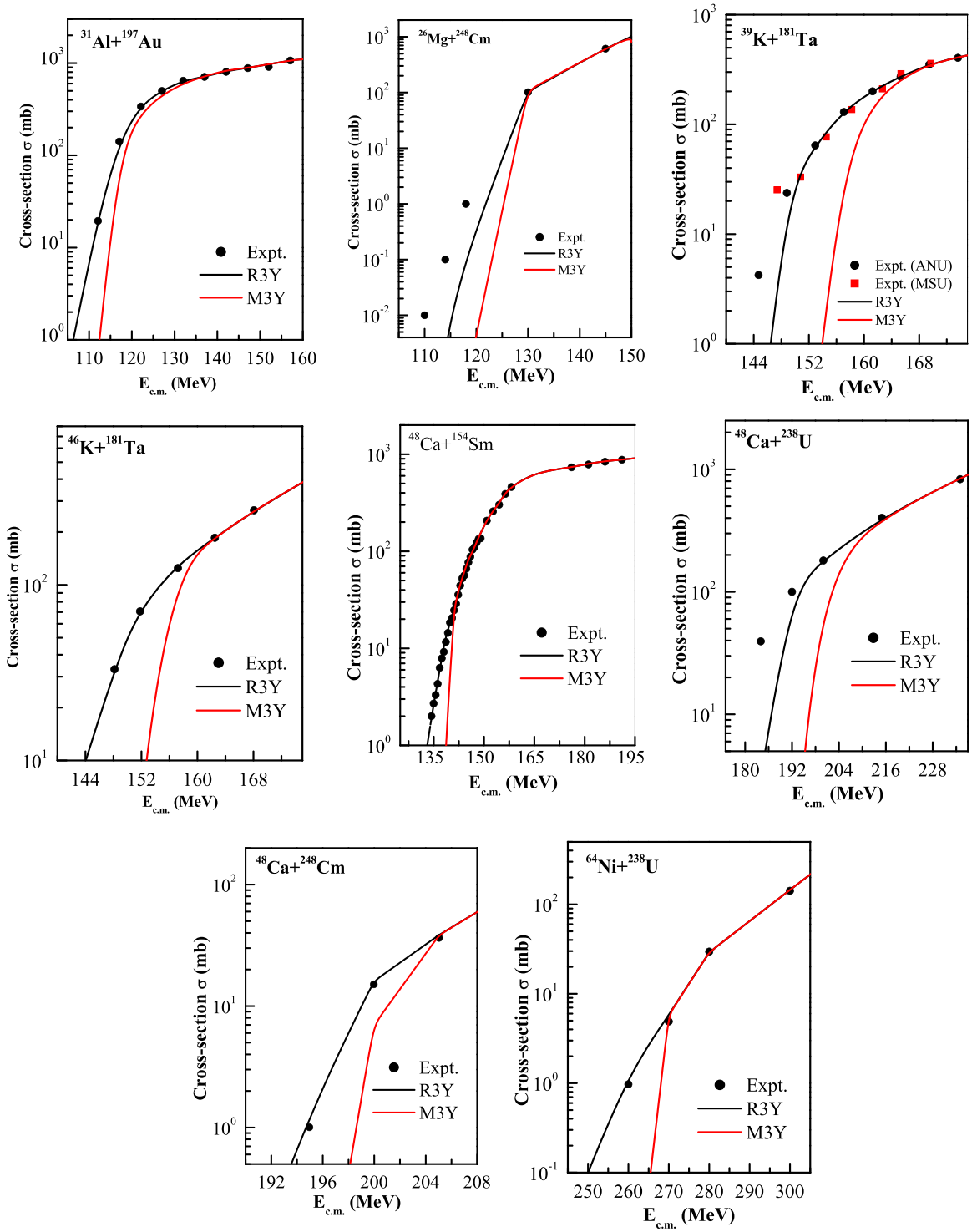

FIG. 4. The fusion cross sections for even-even $^{48}\mathrm{Ca}+^{154}\mathrm{Sm}$, $^{48}\mathrm{Ca}+^{238}\mathrm{U}$, $^{48}\mathrm{Ca}+^{248}\mathrm{Cm}$, $^{64}\mathrm{Ni}+^{238}\mathrm{U}$, $^{26}\mathrm{Mg}+^{248}\mathrm{Cm}$; even-odd $^{46}\mathrm{K}+^{181}\mathrm{Mo}$; and odd-odd $^{31}\mathrm{Al}+^{197}\mathrm{Au}$ and $^{39}\mathrm{K}+^{181}\mathrm{Ta}$ systems using the phenomenological M3Y and relativistic R3Y nucleon-nucleon interaction using the NL3* densities in the ℓ-summed Wong model [74]. The experimental data [33–38] are given for comparison, wherever available. See text for more details.

properties such as deformation, shell correction, and other related observables are reflected in the density distribution and also finally cause the small deviation in the fusion cross sections. More systematic studies will be pursued in the near future.

D. Barrier distribution

The projectile and target need to overcome a barrier to fusion, which arises due to the competition between the long-ranged and repulsive Coulomb force and short-ranged and

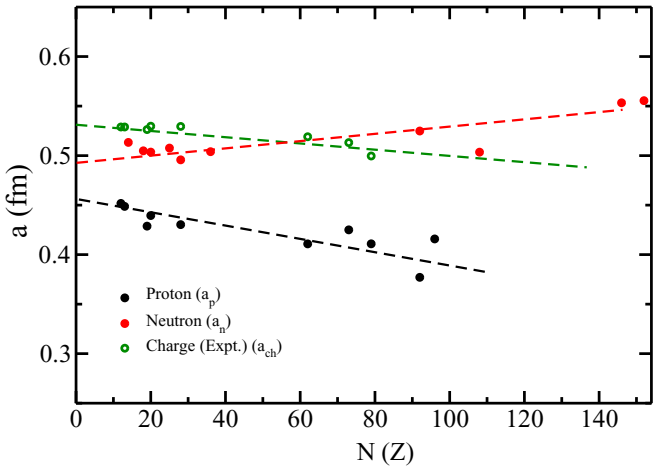

FIG. 5. Values of the equivalent diffuseness parameter are obtained for proton and neutron densities from the relativistic mean field approach for ^{26}Mg, ^{31}Al, ^{39}K, ^{46}K, ^{48}Ca, ^{64}Ni, ^{154}Sm, ^{181}Ta, ^{197}Au, ^{238}U, and ^{248}Cm. The experimental data are obtained for the charge distributions extracted from electron scattering [86,87]. See text for details.

attractive nuclear force. Classically, the transmission probability is a step function at an energy equal to the height of the fusion barrier. The Fermi function blurs the step function into a smoother function, a parabolic barrier. Due to quantum-mechanical tunneling, the barrier height is smeared. The barrier distribution can be extracted from experiment data of fusion cross sections as well. So it is of interest to compare the barrier distribution of theoretical calculations for cross sections with that of the experimental data. The fusion barrier distribution function $[d^2(E\sigma)/dE^2]$ is obtained by differentiating the transmission function with respect to center-of-mass energy. In Fig. 6, we show $d^2(E\sigma)/dE^2$ from fusion excitation functions for the R3Y (black line) and M3Y (red line) interactions. The fusion barrier distribution for the reduced cross sections of the odd-odd $^{31}\mathrm{Al} + {}^{197}\mathrm{Au}$ [Fig. 6(a)], even-odd $^{46}\mathrm{K} + {}^{181}\mathrm{Ta}$ [Fig. 6(b)], even-even $^{48}\mathrm{Ca} + {}^{154}\mathrm{Sm}$ [Fig. 6(c)], and even-even $^{48}\mathrm{Ca} + {}^{238}\mathrm{U}$ [Fig. 6(d)] are given with the experimental data [33–38] for comparison. The barrier distribution corresponding to the experimental data shows a clear signature of nuclear structure at near- and below-barrier energies. Furthermore, one can observe that the behavior of the barrier distribution is sensitive to the choice of interaction potential as well and hence the nuclear

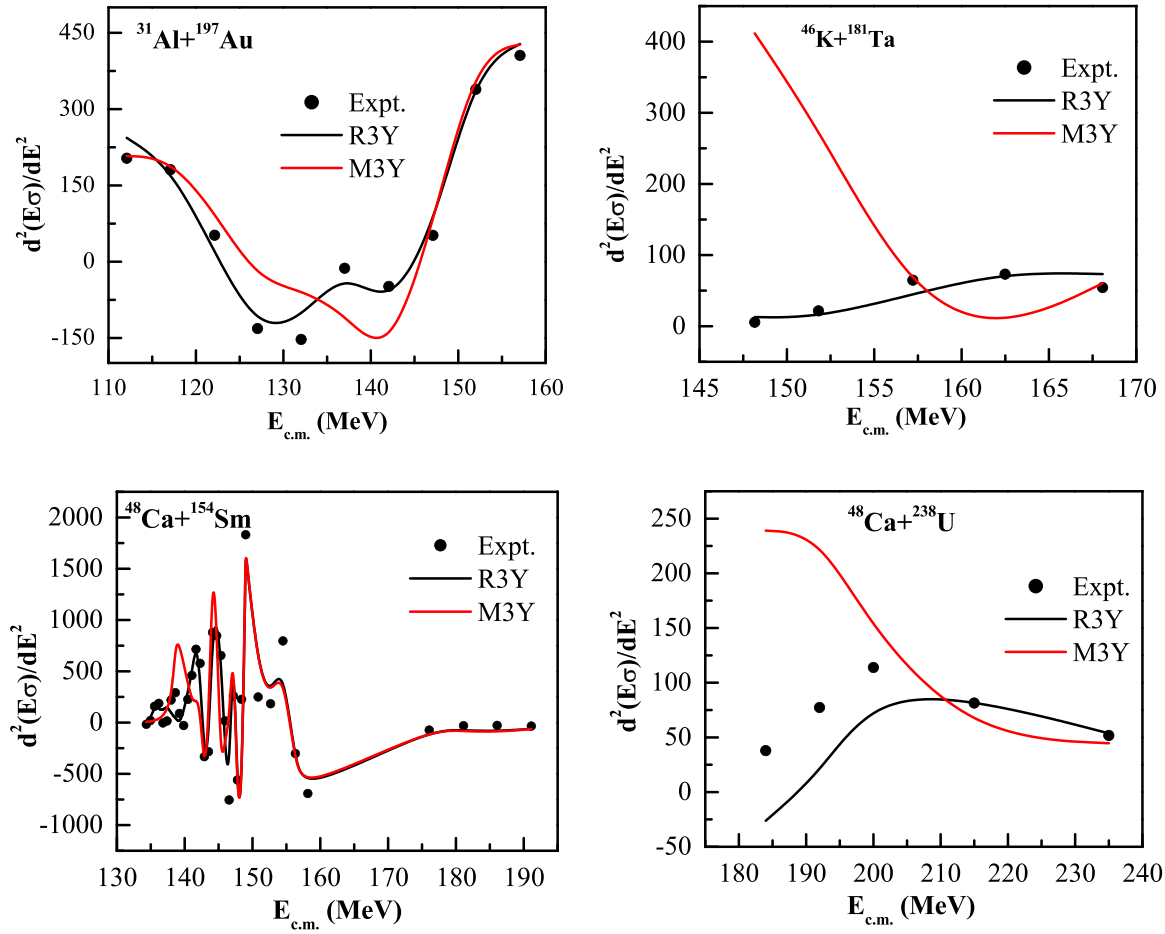

FIG. 6. The barrier distributions for the reactions $^{31}\mathrm{Al} + {}^{197}\mathrm{Au}$, $^{46}\mathrm{K} + {}^{181}\mathrm{Ta}$, $^{48}\mathrm{Ca} + {}^{154}\mathrm{Sm}$, and $^{48}\mathrm{Ca} + {}^{238}\mathrm{U}$ as a function of center-of-mass energy. The experimental values are extracted from the fusion cross section data [33–36] for comparison. See text for details.

structure. This information is a useful tool for understanding the dynamics of subbarrier fusion reactions.

From the figure, we find the $d^2(E\sigma)/dE^2$ values for R3Y are in line with the distribution of barriers extracted from the experimental data for the whole range of energy. The M3Y results fit the data only above the barrier and differ significantly at below-barrier energies. Similar to the predictions of reaction cross sections, here we also find that the results for the barrier-distribution function from R3Y are relatively close to the experimental data for all range of energies, whereas the M3Y fits the data only above barrier energies. One can observes that $d^2(E\sigma)/dE^2$ from R3Y for ^{48}Ca + ^{238}U differs slightly from the experimental data as compared with the other systems, which is also seen in case of the fusion cross section. From the reaction cross sections and barrier distributions, one can conclude that the R3Y interaction produces relatively better agreement than the M3Y potential in comparison with experimental data [33–38]. This can be connected with the barrier energy or height. In other words, the R3Y lowers the barrier significantly as compared with the M3Y case, as shown in Figs. 2 and 3 and in Table I. It is worth mentioning that the step size for energy is large for all the reactions considered except ^{48}Ca + ^{154}Sm. As a result, we get roughened and bumpy (not smoother) curves for the fusion cross sections, as shown in Fig. 4. A reliable barrier distribution can be obtained for a smaller step size of energy, which calls for the experiments for the same. Furthermore, we observe structure effects in the reaction dynamics in terms of the diffuseness parameter, which we will study systematically in the near future. From the above studies, we find an alternative choice for the M3Y *NN* potential, in the relativistic R3Y potential for consistent microscopic studies of fusion properties within double folding procedure. It is worth mentioning that the systems chosen here are combinations of light (projectile) and heavy (target) masses. This implies that the R3Y *NN* potential is applicable for fusion studies for a wide range of mass combinations.

IV. SUMMARY AND CONCLUSIONS

The role of the nucleon-nucleon potential and the nucleon density in the fusion reaction cross section for even-even ^{48}Ca + ^{154}Sm, ^{48}Ca + ^{238}U, ^{48}Ca + ^{248}Cm, ^{64}Ni + ^{238}U, ^{26}Mg + ^{248}Cm; even-odd ^{46}K + ^{181}Ta; and odd-odd ^{31}Al + ^{197}Au and ^{39}K + ^{181}Ta systems, known for fusion hindrance phenomena, is investigated. The fusion-barrier distributions for the reduced fusion cross sections are estimated from the fusion excitation function for the R3Y and the M3Y *NN* interactions. A microscopic approach based on an axial deformed relativistic mean field with the NL3* parameter set is used to obtain the density distribution of projectiles and targets. The relativistic *NN* potential is also obtained for the NL3* parameter set. The ℓ-summed Wong model is used to provide a transparent and analytic calculation of the fusion cross section. We consider the well-known M3Y along with relativistic R3Y *NN* potential to estimate the nuclear interaction potential using NL3* densities within the double-folding method. We determine the effect of the density profile on the fusion cross section in terms of an equivalent diffuseness parameter. The theoretical equivalent diffuseness parameter for the relativistic mean field proton and neutron densities is compared with the experimental diffuseness parameter for the charge density. We find a moderate correlation of structural effects in fusion cross section through the equivalent diffuseness parameter, which requires a systematic study in the near future. Furthermore, a slight lowering in the barrier of the R3Y potential increases the cross section appreciably at energies below the Coulomb barrier. The present analysis again confirms that the R3Y interaction is a better choice than the M3Y interaction for fusion reactions considered over the entire range of barrier energies in predicting the cross section and hence the target-projectile combinations for the synthesis of heavy and superheavy elements.

ACKNOWLEDGMENTS

This work was supported by Board of Research in Nuclear Sciences (BRNS), Department of Atomic Energy (DAE), Govt. of India, Sanction No. 58/14/12/2019-BRNS, FAPESP Projects No. 2014/26195-5 and No. 2017/05660-0, INCT-FNA Project No. 464898/2014-5, and by the CNPq - Brazil.

[1] B. Wang, K. Wen, W.-J. Zhao, E.-G. Zhao, and S.-G. Zhou, At. Data Nucl. Data Tables **114**, 281 (2017).
[2] N. V. Antonenko, E. A. Cherepanov, A. K. Nasirov, V. P. Permjakov, and V. V. Volkov, Phys. Rev. C **51**, 2635 (1995).
[3] G. G. Adamian, N. V. Antonenko, W. Scheid, and V. V. Volkov, Nucl. Phys. A **627**, 361 (1997).
[4] C. H. Dasso, S. Landowne, and A. Winther, Nucl. Phys. A **407**, 221 (1983).
[5] R. A. Broglia, C. H. Dasso, S. Landowne, and A. Winther, Phys. Rev. C **27**, 2433 (1983).
[6] V. I. Zagrebaev, Y. Aritomo, M. G. Itkis, Y. T. Oganessian, and M. Ohta, Phys. Rev. C **65**, 014607 (2001).
[7] M. Liu, N. Wang, Z. Li, X. Wu, and E. Zhao, Nucl. Phys. A **768**, 80 (2006).
[8] L. Zhu, Z.-Q. Feng, C. Li, and F.-S. Zhang, Phys. Rev. C **90**, 014612 (2014).
[9] R. Kumar, J. A. Lay, and A. Vitturi, Phys. Rev. C **89**, 027601 (2014).
[10] M. Bhuyan and R. Kumar, Phys. Rev. C **98**, 054610 (2018).
[11] D. Jain, R. Kumar, and M. K. Sharma, Nucl. Phys. A **915**, 106 (2013).
[12] R. Kumar, M. K. Sharma, and R. K. Gupta, Nucl. Phys. A **870**, 42 (2011).
[13] S. Hofmann *et al.*, Z. Phys. A: Hadrons Nucl. **350**, 277 (1995).
[14] S. Hofmann *et al.*, Z. Phys. A: Hadrons Nucl. **354**, 229 (1996).
[15] S. Hofmann *et al.*, Rep. Prog. Phys. **61**, 639 (1998).
[16] Yu. Ts. Oganessian *et al.*, Nucl. Phys. A **685**, 17c (2001).
[17] Yu. Ts. Oganessian *et al.*, Phys. Rev. C **69**, 021601(R) (2004).
[18] Yu. Ts. Oganessian, J. Phys. G **34**, R165 (2007).
[19] Yu. Ts. Oganessian *et al.*, Phys. Rev. Lett. **104**, 142502 (2010).
[20] Yu. Ts. Oganessian *et al.*, Phys. Rev. C **83**, 054315 (2011).

[21] A. Marinov, I. Rodushkin, Y. Kashiv, L. Halicz, I. Segal. A. Pape, R. V. Gentry, H. W. Miller, D. Kolb, and R. Brandt, Phys. Rev. C **76**, 021303(R) (2007).

[22] A. Marinov, I. Rodushkin, A. Pape, Y. Kashiv, D. Kolb, R. Brandt, R. V. Gentry, H. W. Miller, L. Halicz, and I. Segal, Int. J. Mod. Phys. E **18**, 621 (2009).

[23] S. Hofmann and G. Mũnzenberg, Rev. Mod. Phys. **72**, 733 (2000).

[24] S. G. Steadman and M. J. Rhoades-Brown, Annu. Rev. Nucl. Part. Sci. **36**, 649 (1986).

[25] M. Beckerman, Rep. Prog. Phys. **51**, 1047 (1988).

[26] H. J. Krappe, K. Mõhring, M. C. Nemes, and H. Z. Rossner, J. Phys. A Atoms and Nuclei **314**, 23 (1983).

[27] N. Rowley, G. R. Satchler, and P. H. Stelson, Phys. Lett. B **254**, 25 (1991).

[28] M. Dasgupta, D. J. Hinde, N. Rowley, and A. M. Stefanini, Annu. Rev. Nucl. Part. Sci. **48**, 401 (1998).

[29] B.-A. Bian, F.-S. Zhang, and H.-Y. Zhou, Nucl. Phys. A **829**, 1 (2009).

[30] V. V. Sargsyan, A. S. Zubov, G. G. Adamian, N. V. Antonenko, and S. Heinz, Phys. Rev. C **88**, 054609 (2013).

[31] V. V. Sargsyan, G. G. Adamian, N. V. Antonenko, and Z. Kohley, Phys. Rev. C **92**, 054613 (2015).

[32] X. J. Bao, Y. Gao, J. Q. Li, and H. F. Zhang, Phys. Rev. C **93**, 044615 (2016).

[33] Y. X. Watanabe *et al.*, Eur. Phys. J. A **10**, 373 (2001).

[34] G. N. Knyazheva *et al.*, Phys. Rev. C **75**, 064602 (2007).

[35] E. V. Prokhorova *et al.*, in *Proceedings of the International Symposium on Exotic Nuclei (EXON2004), Peterhof, Russian Federation, July 52, 2004*, edited by Y. E. Penionzhkevich and E. A. Cherepanov (World Scientific, Singapore, 2005), p. 325.

[36] M. G. Itkis *et al.*, Nucl. Phys. A **734**, 136 (2004).

[37] E. M. Kozulin *et al.*, Phys. Lett. B **686**, 227 (2010).

[38] A. Wakhle, K. Hammerton, Z. Kohley, D. J. Morrissey, K. Stiefel, J. Yurkon, J. Walshe, K. J. Cook, M. Dasgupta, D. J. Hinde *et al.*, Phys. Rev. C **97**, 021602(R) (2018).

[39] V. V. Sargsyan, Z. Kanokov, G. G. Adamian, N. V. Antonenko, and W. Scheid, Phys. Rev. C **80**, 034606 (2009).

[40] R. Kumar, Phys. Rev. C **86**, 044612 (2012).

[41] R. Vandenbosch, Annu. Rev. Nucl. Part. Sci. **42**, 447 (1992).

[42] A. B. Balantekin and N. Takigawa, Rev. Mod. Phys. **70**, 77 (1998).

[43] K. W. Mc Voy and M. E. Brandan, Nucl. Phys. A **542**, 295 (1992).

[44] M. E. Brandan and G. R. Satchler, Phys. Rep. **285**, 143 (1997).

[45] Y. Kondõ, M. E. Brandan, and G. R. Satchler, Nucl. Phys. A **637**, 175 (1998).

[46] G. R. Satchler and W. G. Love, Phys. Rep. **55**, 183 (1979).

[47] B. B. Singh, M. Bhuyan, S. K. Patra, and R. K. Gupta, J. Phys. G **39**, 025101 (2012).

[48] B. B. Sahu, S. K. Singh, M. Bhuyan, S. K. Biswal, and S. K. Patra, Phys. Rev. C **89**, 034614 (2014).

[49] M. Bhuyan, *Properties of Finite Nuclei using Effective Interaction: Structure of Drip-Line and Super-Heavy Nuclei in Effective Relativistic and Nonrelativistic Interactions* (LAP Lambert Academic Publishing, Saarbrücken, Germany, 2014).

[50] D. J. Hinde and M. Dasgupta, AIP Conf. Proc. **425**, 233 (1998).

[51] M. Dutra, O. Lourenço, S. S. Avancini, B. V. Carlson, A. Delfino, D. P. Menezes, C. Providência, S. Typel, and J. R. Stone, Phys. Rev. C **90**, 055203 (2014).

[52] J. Boguta and A. R. Bodmer, Nucl. Phys. A **292**, 413 (1977).

[53] B. D. Serot and J. D. Walecka, in *Advances in Nuclear Physics*, edited by J. W. Negele and E. Vogt (Plenum Press, New York, 1986), Vol. 16, p. 1.

[54] W. Pannert, P. Ring, and J. Boguta, Phys. Rev. Lett. **59**, 2420 (1987).

[55] S. K. Singh, M. Bhuyan, P. K. Panda, and S. K. Patra, J. Phys. G **40**, 085104 (2013).

[56] S. K. Singh, S. K. Biswal, M. Bhuyan, and S. K. Patra, J. Phys. G **41**, 055201 (2014).

[57] M. Bhuyan, Phys. Rev. C **92**, 034323 (2015).

[58] M. Bhuyan, B. V. Carlson, S. K. Patra, and S.-G. Zhou, Phys. Rev. C **97**, 024322 (2018).

[59] M. Bhuyan, Phys. At. Nucl. **81**, 15 (2018).

[60] G. A. Lalazissis, S. Raman, and P. Ring, At. Data Nucl. Data Tables **71**, 1 (1999).

[61] P.-G. Reinhard, Rep. Prog. Phys. **52**, 439 (1989).

[62] P. Ring, Prog. Part. Nucl. Phys. **37**, 193 (1996).

[63] D. Vretenar, A. V. Afanasjev, G. A. Lalazissis, and P. Ring, Phys. Rep. **409**, 101 (2005).

[64] J. Meng, H. Toki, S. G. Zhou, S. Q. Zhang, W. H. Long, and L. S. Geng, Prog. Part. Nucl. Phys. **57**, 470 (2006).

[65] N. Paar, D. Vretenar, and G. Colo, Rep. Prog. Phys. **70**, 691 (2007).

[66] M. Bhuyan, S. K. Patra, and R. K. Gupta, Phys. Rev. C **84**, 014317 (2011).

[67] X.-F. Zhao and H.-Y. Jia, Phys. Rev. C **85**, 065806 (2012).

[68] G. A. Lalazissis, S. Karatzikos, R. Fossion, D. Pena Arteaga, A. V. Afanasjev, and P. Ring, Phys. Lett. B **671**, 36 (2009).

[69] L. I. Schiff, Phys. Rev. **84**, 10 (1951); **83**, 252 (1951).

[70] L. I. Schiff, Phys. Rev. **84**, 1 (1951).

[71] J. Dobaczewski, H. Flocard, and J. Treiner, Nucl. Phys. A **422**, 103 (1984).

[72] D. G. Madland and J. R. Nix, Nucl. Phys. A **476**, 1 (1981).

[73] C. Y. Wong, Phys. Rev. Lett. **31**, 766 (1973).

[74] R. Kumar, M. Bansal, S. K. Arun, and R. K. Gupta, Phys. Rev. C **80**, 034618 (2009).

[75] M. Beckerman, J. Ball, H. Enge, M. Salomaa, A. Sperduto, S. Gazes, A. DiRienzo, and J. D. Molitoris, Phys. Rev. C **23**, 1581 (1981).

[76] D. L. Hill and J. A. Wheeler, Phys. Rev. **89**, 1102 (1953).

[77] T. D. Thomas, Phys. Rev. **116**, 703 (1959).

[78] N. Rowley and K. Hagino, Phys. Rev. C **91**, 044617 (2015).

[79] N. W. Lwin, N. N. Htike, and K. Hagino, Phys. Rev. C **95**, 064601 (2017).

[80] A. J. Toubiana, L. F. Canto, and M. S. Hussein, Braz. J. Phys. **47**, 321 (2017).

[81] S. Weinberg, Phys. A (Amsterdam, Neth.) **96**, 327 (1979).

[82] D. B. Kaplan, M. J. Savage, and M. B. Wise, Nucl. Phys. B **534**, 329 (1998).

[83] U. van Kolck, Prog. Part. Nucl. Phys. **43**, 337 (1999).

[84] E. Epelbaum, H.-W. Hammer and Ulf-G. Meißner, Rev. Mod. Phys. **81**, 1773 (2009).

[85] A. Ekström, G. Baardsen, C. Forssén, G. Hagen, M. Hjorth-Jensen, G. R. Jansen, R. Machleidt, W. Nazarewicz, T. Papenbrock, J. Sarich, and S. M. Wild, Phys. Rev. Lett. **110**, 192502 (2013).

[86] H. De Vries, C. W. De Jager, and C. De Vries, At. Data Nucl. Data Tables **36**, 495 (1987).

[87] E. G. Nadjakov, K. P. Marinova, and Y. P. Gangrsky, At. Data Nucl. Data Tables **56**, 133 (1994).